ISSN 1674-1056
http://cpb.iphy.ac.cn
http://iopscience.iop.org/cpb
中国物理 B
Chinese Physics
中国物理 Chinese Physics B

## GO-based ray field tracing method for complex source beam applications

Min Gao(高敏), Feng Yang(杨峰), Xue-Wu Cui(崔学武), Rui Wang(王瑞)
**Citation:**Chin. Phys. B . 2018, 27(4): 040401. **doi:** 10.1088/1674-1056/27/4/040401

Journal homepage: http://cpb.iphy.ac.cn; http://iopscience.iop.org/cpb

**What follows is a list of articles you may be interested in**

---

## Design of scale model of plate-shaped absorber in wide frequency range

Li-Ming Yuan(袁黎明), Yong-Gang Xu(许勇刚), Wei Gao(高伟), Fei Dai(戴飞), Qi-Lin Wu(吴琪琳)
Chin. Phys. B . 2018, 27(4): 044101. **doi:** 10.1088/1674-1056/27/4/044101

## A broadband cross-polarization conversion anisotropic metasurface based on multiple plasmon resonances

M Ismail Khan, Farooq A Tahir
Chin. Phys. B . 2018, 27(1): 014101. **doi:** 10.1088/1674-1056/27/1/014101

## Ultra-broadband and polarization-independent planar absorber based on multilayered graphene

Jiao Wang(王娇), Chao-Ning Gao(高超宁), Yan-Nan Jiang(姜彦南), Charles Nwakanma Akwuruoha
Chin. Phys. B . 2017, 26(11): 114102. **doi:** 10.1088/1674-1056/26/11/114102

## An electrically tunable metasurface integrated with graphene for mid-infrared light modulation

Zongpeng Wang(王宗鹏), Ya Deng(邓娅), LianFeng Sun(孙连峰)
Chin. Phys. B . 2017, 26(11): 114101. **doi:** 10.1088/1674-1056/26/11/114101

## High-frequency gravitational waves having large spectral densities and their electromagnetic response

Li Fang-Yu, Wen Hao, Fang Zhen-Yun
Chin. Phys. B . 2013, 22(12): 120402. **doi:** 10.1088/1674-1056/22/12/120402

---

# Geometrical optics-based ray field tracing method for complex source beam applications*

Min Gao(高敏), Feng Yang(杨峰)†, Xue-Wu Cui(崔学武), and Rui Wang(王瑞)

*School of Electronic Engineering, University of Electronic Science and Technology of China, Chengdu* 611731, *China*

(Received 21 September 2017; revised manuscript received 6 December 2017; published online 10 March 2018)

Due to the fact that traditional ray field tracking approaches require a large number of geometrical optical (GO) ray tubes, they are very inefficient in many practical applications. An improved ray model scheme for a complex source beam (CSB) tracking technique is proposed in this paper. The source field can be expressed by a superposition of CSBs, then every CSB basis function has a Gaussian-type amplitude distribution and is suitable for replacing a GO ray tube in the ray tracing approach. The complex phase matching technique is adopted to find the reflected beam in the reflection point where local approximation is used to represent the curved surface in its neighborhood. A new solution to multiple reflections using the conventional right-handed reflected system is used to track the field easily. Numerical results show the accuracy of the proposed method.

**Keywords:** complex source beam, complex phase matching, local approximation, multiple reflection

**PACS:** 04.30.Nk, 41.20.Jb, 42.15.Dp **DOI:** 10.1088/1674-1056/27/4/040401

## 1. Introduction

With the demand for higher data rates and mobility, there has been an unprecedented growth in the development and deployment of wireless communication systems. Understanding radio channel path characteristics is a very important factor for ensuring the quality of service and high data rates for wireless communication systems.[1] Two different approaches are generally used to predict the electric field strength. Empirical models,[2,3] based on the regression of the data gained in measurement, are very fast but not very accurate. Nevertheless, these problems can be avoided by deterministic models. The ray-optical model[4,5] serves as a representative one among them. The ray tracing based on the uniform geometrical theory of diffraction (UTD) is widely used to estimate a site-specific radio propagation for wireless applications.[6,7] When ray tracing is used to calculate the field intensity distribution, each ray will perform the receiving ball algorithm to determine whether the receiver receives the contribution of the ray.[8] Then the total field at the desired observation position can be obtained via the superposition of all contributions from those rays received by the ball. This ray-optical method requires a very large number of GO rays and hence becomes inefficient in many practical applications.

The complex source beam (CSB) idea provides a very efficient tool to estimate the fields radiated by sources. Actually, CSB is a space-time Green's function in complex space. A field excited by any source can then be constructed by CSB.[9] This CSB basis function has a Gaussian-type amplitude distribution and is suitable for replacing the GO ray-optical model in the ray tracing approach because the Gaussian-type distribution tends to yield a more efficient field expansion. Then a new ray tracing method with spectral features of CSB can be used to analyze the wave propagation characteristics of the environment. The CSB basis function provides a solution which maintains the advantages of the GO ray-optical model, and on the other hand, it tends to overcome their shortcomings. Using an additional Gaussian amplitude taper to confine its energy distribution, the CSB modified the traditional GO ray tube to make it wider. The collective treatment of the receiving points uses the CSB formulas which provides field-coverage values at any point in a straightforward manner without reception sphere. Therefore, the CSB is an appropriate candidate for field estimation.

For a complex environment assessment, it often contains a variety of targets. Plane surface meshes have been generally used to represent these complex objects. When a CSB illuminates on a plane interface, the reflected and transmitted fields can be expressed in the form of CSBs by phase matching process.[10,11] For a curved surface, the corresponding curvature information will be totally dropped if the model is discretized with the plane interface. It can be assumed that the radius of the surface curvature is electrically large and varies so slowly that the reflected field may be assumed to be a CSB in the paraxial region and its parameters can be found by complex phase matching of the incident and reflected beams on the surface. This complex phase matching yields a complex reflected caustic distance in complex space, which is similar

*Project supported by the National Natural Science Foundation of China (Grant Nos. 61301056 and 61231001), the Fundamental Research Funds for the Central Universities, China (Grant No. ZYGX2014J012), the Fok Ying Tung Education Foundation, China (Grant No. 141062), the Aero-Science Fund, China (Grant No. 20142580012), and the "111" Project (Grant No. B07046).

†Corresponding author. E-mail: yangf@uestc.edu.cn

© 2018 Chinese Physical Society and IOP Publishing Ltd 

to the GO caustic distance in real space. While the caustic problem in complex space will not cause the same singularity problem as experienced in GO in the real space.

In this paper, an improved ray model scheme for CSB tracking is presented. Local approximation as a paraboloid in the neighborhood of the reflection point is adopted to represent the curved surface in the environment. The complex phase matching technique provides an efficient way to find the reflected CSB, which is especially useful for tracking a CSB through multiple reflections within the framework of complex ray theory. A new solution for the reflection of a CSB using the conventional right-handed reflected system will be developed in this paper, which can be easily employed in existing computer codes which track a GO ray field, and it is very useful for the multiple reflections.

## 2. Paraxial CSB and astigmatic GO ray field

The CSB concept is utilized to efficiently treat a class of electromagnetic (EM) radiation and scattering problems. The paraxial representation of the CSB, which is given in Ref. [9], is repeated as follows:

$$\frac{\mathrm{e}^{-\mathrm{j}k\tilde{R}}}{\tilde{R}} = \frac{1}{z+\mathrm{j}b}\mathrm{e}^{kb}\exp\left[-\mathrm{j}kz\left(1+\frac{1}{2}\left(\frac{\rho^2}{z^2+b^2}\right)\right)\right] \times \exp\left[-\frac{1}{2}kb\frac{\rho^2}{z^2+b^2}\right]. \quad (1)$$

As depicted in Ref. [12], the CSB behaves like a rotationally symmetric Gaussian beam (GB) in its paraxial region. A comparison of the source free ray optical GB with the CSB shows that the only difference is that the source free GB does not contain the factor $\mathrm{e}^{kb}$, but has a factor of $\mathrm{j}b$. Since CSB (or GB) is just treated as a basis function, weight coefficients $C_m(\omega)$ need adding when dealing with sources as presented in Ref. [9], we can directly use some existing conclusions from the perspective of GB. A $z$-propagating radiated GB can be obtained by analytically extending the real GO ray field into the complex domain, as depicted in Fig. 1.

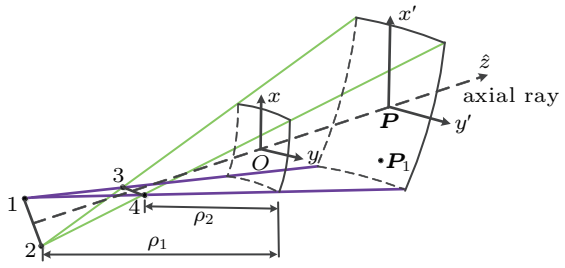



**Fig. 1.** (color online) Real ray tube propagation.

Let $E(\boldsymbol{P}_1)$ be the electric field at point $\boldsymbol{P}$, and it can be expressed as

$$E(\boldsymbol{P}_1) = E(0)\sqrt{\frac{\det\tilde{\boldsymbol{Q}}(\boldsymbol{P})}{\det\tilde{\boldsymbol{Q}}(0)}}\exp\left\{-\mathrm{j}k\left[z+\frac{1}{2}\boldsymbol{\rho}^{\mathrm{T}}\tilde{\boldsymbol{Q}}(\boldsymbol{P})\boldsymbol{\rho}\right]\right\}, \quad (2)$$

where $\det\tilde{\boldsymbol{Q}}(\boldsymbol{P})$ denotes the determinant of matrix $\tilde{\boldsymbol{Q}}(\boldsymbol{P})$ and $\boldsymbol{\rho}^{\mathrm{T}} = (xy)$. Point $\boldsymbol{P}_1$ is located on the phasefront centered at point $\boldsymbol{P}$. The complex phase matrix $\tilde{\boldsymbol{Q}}$ is the curvature matrix $\boldsymbol{Q}$ expressed in complex domain, which is defined as follows:

$$\boldsymbol{Q}(z) = \begin{bmatrix} \frac{1}{z+\rho_1} & 0 \\ 0 & \frac{1}{z+\rho_2} \end{bmatrix},$$
$$\tilde{\boldsymbol{Q}}(z) = \begin{bmatrix} \frac{1}{z+\mathrm{j}b_1} & 0 \\ 0 & \frac{1}{z+\mathrm{j}b_2} \end{bmatrix}, \quad (3)$$

where $z+\rho_1$ and $z+\rho_2$ are the caustic distances (or wavefront radii of curvature) as shown in Fig. 1, $z+\mathrm{j}b_1$ and $z+\mathrm{j}b_2$ are their complex domain forms. If $\tilde{\boldsymbol{Q}}(z)$ is a diagonal matrix, the main diagonal elements are the complex principal curvatures, and $\boldsymbol{\rho}^{\mathrm{T}} = (xy)$ is the eigenvector corresponding to the principal complex curvature direction of the beam wavefront. Unlike the applications of GO which are limited to a ray technique associated with possible ray caustics in real space, it is quiet convenient that the complex caustic will not lead to the same singularity problem in complex space. When the complex caustic distances are selected to be equal, i.e., $b_1 = b_2 = b$, where $b$ is the beam parameter which is defined as beam collimation distance,[12] such that

$$E(\boldsymbol{P}_1) = E(0)\frac{\mathrm{j}b}{z+\mathrm{j}b}\exp\left\{-\mathrm{j}k\left[z+\frac{1}{2}\frac{\rho^2}{z+\mathrm{j}b}\right]\right\} = E(0)\frac{\mathrm{j}b}{z+\mathrm{j}b}\exp\left[-\mathrm{j}kz\left(1+\frac{1}{2}\frac{\rho^2}{z^2+b^2}\right)\right] \times \exp\left[-\frac{1}{2}kb\frac{\rho^2}{z^2+b^2}\right]. \quad (4)$$

Equation (4) has a similar form to Eq. (1), which is especially useful in tracking a CSB through multiple reflections within the framework of complex ray theory.

## 3. Wave propagation at point of reflection

The CSB behaves like a rotationally symmetric GB where $b_1 = b_2 = b$ in its paraxial region. Each CSB basis incident electric field which is expanded by sources has a Gaussian-type amplitude distribution and can be expressed as

$$\boldsymbol{E}_i(x_i,y_i,z_i) = \boldsymbol{E}_i^0\sqrt{\frac{\det\tilde{\boldsymbol{Q}}_i(z_i)}{\det\tilde{\boldsymbol{Q}}_i(0)}} \times \exp\left\{-\mathrm{j}k\left[z_i+\frac{1}{2}\boldsymbol{\rho}_i^{\mathrm{T}}\tilde{\boldsymbol{Q}}_i(z_i)\boldsymbol{\rho}_i\right]\right\}, \quad (5)$$

where $(x_i,y_i,z_i)$ is the coordinate system of the incident beam and $\tilde{\boldsymbol{Q}}_i(z_i)$ is the complex phase matrix with $\boldsymbol{Q}_{11}^i = \boldsymbol{Q}_{22}^i = 1/(z+\mathrm{j}b)$ and $\boldsymbol{Q}_{12}^i = \boldsymbol{Q}_{21}^i = 0$. When the incident beam is

well focused, $b$ must be large enough such that the most important contribution to the reflection is in the neighborhood of the reflection point, which in general will have the form of an astigmatic Gaussian-type beam. The origin of the coordinate system $(x_i, y_i, z_i)$ here is selected to coincide with the origin of the reflection surface coordinate system such that $\boldsymbol{E}_i^0$ denotes the field of incident beam at the point of reflection and $\tilde{\boldsymbol{Q}}_i(0)$ denotes the complex phase matrix at the point of beam reflection. The coordinate transformation between $(x_i, y_i, z_i)$ and the reflection surface coordinates $(x, y, z)$ can be expressed as

$$\begin{bmatrix} x_i \\ y_i \\ z_i \end{bmatrix} = \begin{bmatrix} c_{11} & c_{12} & c_{13} \\ c_{21} & c_{22} & c_{23} \\ c_{31} & c_{32} & c_{33} \end{bmatrix} \begin{bmatrix} x \\ y \\ z \end{bmatrix}. \tag{6}$$

Then the reflected field can be expressed as the form of an astigmatic Gaussian beam form

$$\begin{aligned} \boldsymbol{E}_r(x_r, y_r, z_r) &= \boldsymbol{E}_r^0 \sqrt{\frac{\det \tilde{\boldsymbol{Q}}_r(z_r)}{\det \tilde{\boldsymbol{Q}}_r(0)}} \\ &\quad \times \exp\left\{-\mathrm{j}k\left[z_r + \frac{1}{2}\boldsymbol{\rho}_r^{\mathrm{T}} \tilde{\boldsymbol{Q}}_r(z_r)\boldsymbol{\rho}_r\right]\right\}, \end{aligned} \tag{7}$$

where $(x_r, y_r, z_r)$ is the reflection beam coordinate system and $\tilde{\boldsymbol{Q}}_r(z_r)$ is the corresponding complex phase $\boldsymbol{Q}$ matrix of the reflected beam. It is also convenient to select the origin of the coordinate system $(x_r, y_r, z_r)$ to coincide with the origin of the reflection surface coordinate system such that $\boldsymbol{E}_r^0$ denotes the field of reflected beam at the point of reflection and $\tilde{\boldsymbol{Q}}_r(0)$ denotes the complex phase matrix at the point of beam reflection. Then the phase matching approach can be used here to yield the relationship[11]

$$\boldsymbol{\Theta}_r^{\mathrm{T}} Q_r(0) \boldsymbol{\Theta}_r = \boldsymbol{\Theta}_i^{\mathrm{T}} Q_i(0) \boldsymbol{\Theta}_i + 2C_0 \cos\theta_i, \tag{8}$$

where

$$\boldsymbol{\Theta}_i = \begin{bmatrix} \hat{x}_i \cdot \hat{x} & \hat{x}_i \cdot \hat{y} \\ \hat{y}_i \cdot \hat{x} & \hat{y}_i \cdot \hat{y} \end{bmatrix} = \begin{bmatrix} c_{11} & c_{12} \\ c_{21} & c_{22} \end{bmatrix}, \quad \boldsymbol{\Theta}_r = \begin{bmatrix} \hat{x}_r \cdot \hat{x} & \hat{x}_r \cdot \hat{y} \\ \hat{y}_r \cdot \hat{x} & \hat{y}_r \cdot \hat{y} \end{bmatrix}, \tag{9}$$

here the superscript T refers to the transpose matrix, $\theta_i$ is the angle between the incident beam axis and the normal direction of the surface at the reflection point, and $C_0$ denotes the curvature matrix at the reflection point on the surface. The local approximation is used to obtain the curvature matrix, and the conventional right-handed reflected system is used to track the field easily, which will be accounted for separately.

### 3.1. Local approximation of surface

Consider an arbitrary curved surface, its equation can be expressed as

$$\boldsymbol{r} = \boldsymbol{r}(u, v), \tag{10}$$

where $u$, $v$ denote the surface coordinate parameters. In the vicinity of $\boldsymbol{r}_0$, the surface can be expanded in a power series form as follows:

$$\begin{aligned} \boldsymbol{r} &= \boldsymbol{r}_0 + \boldsymbol{r}_u \mathrm{d}u + \boldsymbol{r}_v \mathrm{d}v \\ &\quad + \frac{1}{2}(\boldsymbol{r}_{uu}\mathrm{d}u^2 + 2\boldsymbol{r}_{uv}\mathrm{d}u\mathrm{d}v + \boldsymbol{r}_{vv}\mathrm{d}v^2) + \mathrm{O}(\mathrm{d}s^3), \end{aligned} \tag{11}$$

where $\boldsymbol{r}_u, \boldsymbol{r}_v$ and $\boldsymbol{r}_{uu}, \boldsymbol{r}_{uv}, \boldsymbol{r}_{vv}$ are the first and second order partial derivatives of $u, v$, $\mathrm{d}S^2 = \mathrm{d}u^2 + \mathrm{d}v^2$. We define the unit normal vector $\hat{n}$ at the point $\boldsymbol{r}_0$, it is noted that $\boldsymbol{r}_u \perp \hat{n}, \boldsymbol{r}_v \perp \hat{n}$, then

$$\begin{aligned} (\boldsymbol{r} - \boldsymbol{r}_0) \cdot \hat{n} &= \frac{1}{2}(L\mathrm{d}u^2 + 2M\mathrm{d}u\mathrm{d}v + N\mathrm{d}v^2) + \mathrm{O}(\mathrm{d}s^3) \\ &= \frac{1}{2}(\mathrm{d}u\mathrm{d}v)\begin{pmatrix} L & M \\ M & N \end{pmatrix}\begin{pmatrix} \mathrm{d}u \\ \mathrm{d}v \end{pmatrix} + \mathrm{O}(\mathrm{d}s^3). \end{aligned} \tag{12}$$

If $\boldsymbol{r}_0$ is selected to be the origin of the surface coordinate system, the surface can be expressed as

$$n = -\frac{1}{2}(\boldsymbol{t})^{\mathrm{T}} C_0 \boldsymbol{t}, \tag{13}$$

where

$$n = -\boldsymbol{r} \cdot \hat{n}, \quad C_0 = \begin{pmatrix} L & M \\ M & N \end{pmatrix}, \quad \boldsymbol{t} = (u, v)^{\mathrm{T}} \tag{14}$$

with $C_0$ here determining the curvature matrix at the reflection point on the surface. For convenience, it is assumed that the surface may be locally approximated by a paraboloid in the neighborhood of the reflection point which is given by

$$\begin{aligned} z &= -\frac{1}{2}\left(\frac{x^2}{R_1} + \frac{y^2}{R_2}\right) \\ &= -\frac{1}{2}(x, y)\begin{pmatrix} 1/R_1 & 0 \\ 0 & 1/R_2 \end{pmatrix}(x, y)^{\mathrm{T}}, \end{aligned} \tag{15}$$

where $R_1$ and $R_2$ are the local principal radii of curvature of the surface in the $x$ and $y$ directions, respectively.

### 3.2. Simple rule for multi-reflections

It is noted that for a well focused CSB, the magnitude of the beam will die out exponentially outside the paraxial region, which implies that the reflected beam is generated primarily by the surface within this region. The complex phase matching technique is presented here to find the reflected beam, which is especially useful in tracking a CSB through multiple reflections. As depicted in Ref. [11], the reflected field can be found via the phase matching method. The reflected coordinate system is chosen to mirror the incident coordinate system at the reflection point such that $\boldsymbol{\Theta}_r$ is equivalent to $\boldsymbol{\Theta}_i$. However, the reflected coordinate system will become left-handed, which is contrary to the conventional right-hand rule for a coordinate system, and it is not convenient to track the ray field through multiple reflections. Figure 2(a) shows that the alternative choice for the reflected beam is obtained from

$$\begin{cases} \hat{x}_r = \hat{x}_i - 2(\hat{x}_i \cdot \hat{z})\hat{z}, \\ \hat{y}_r = -\hat{y}_i + 2(\hat{y}_i \cdot \hat{z})\hat{z}, \\ \hat{z}_r = \hat{z}_i - 2(\hat{z}_i \cdot \hat{z})\hat{z}. \end{cases} \tag{16}$$

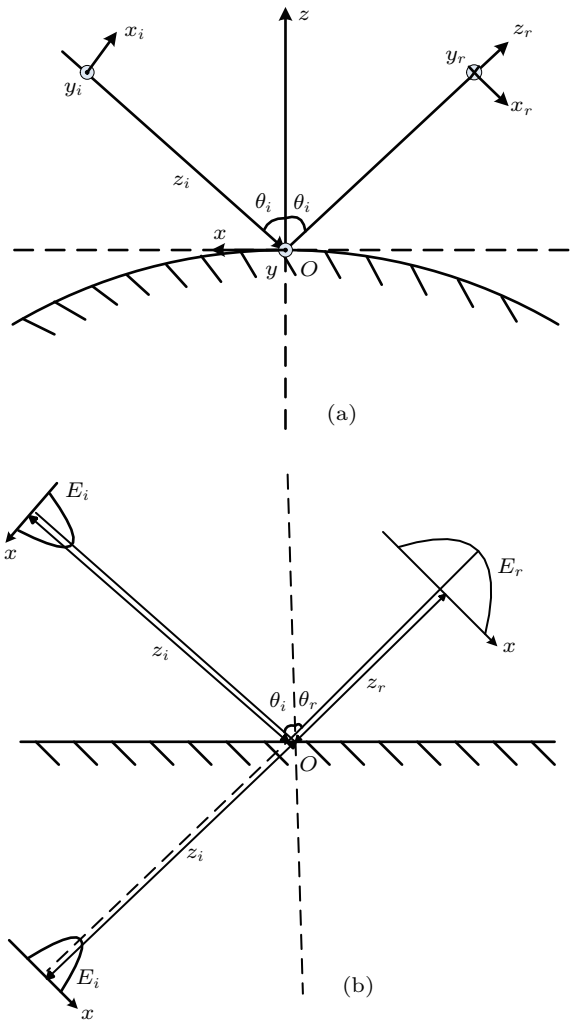



**Fig. 2.** Beam reflection from the surface, showing (a) curved surface and (b) flat structure.

This choice of $(x_r, y_r, z_r)$ provides a very efficient means of beam tracking since one can just track the complex phase $\boldsymbol{Q}$ matrix. Since the reflected coordinate system is chosen to be the conventional right-hand rule, it follows that $\Theta_r$ is not equal to $\Theta_i$, and it turns out that $\det(\Theta_r) = -\det(\Theta_i)$. Then equation (8) can be solved for $\boldsymbol{Q}_r(0)$ as

$$\begin{aligned}\boldsymbol{Q}_r(0) \;=\; & (\Theta_r^{\mathrm{T}})^{-1}\Theta_i^{\mathrm{T}}\boldsymbol{Q}_i(0)\Theta_i(\Theta_r)^{-1} \\ & +2\cos\theta_i(\Theta_r^{\mathrm{T}})^{-1}C_0(\Theta_r)^{-1}. \end{aligned} \tag{17}$$

It is noted that $\boldsymbol{Q}_i(0)$ can be obtained by CSB expansion, and has been expressed in Section 3. Then one can explicitly determine the elements of the $\boldsymbol{Q}_r(0)$ as

$$Q^r_{11} = Q^i_{11} + \frac{2}{\cos\theta_i}\left(\frac{c_{22}^2}{R_1} + \frac{c_{21}^2}{R_2}\right), \tag{18}$$

$$Q^r_{12} = Q^r_{21} = -Q^i_{12} + \frac{2}{\cos\theta_i}\left(\frac{c_{22}c_{12}}{R_1} + \frac{c_{11}c_{21}}{R_2}\right), \tag{19}$$

$$Q^r_{22} = Q^i_{22} + \frac{2}{\cos\theta_i}\left(\frac{c_{12}^2}{R_1} + \frac{c_{11}^2}{R_2}\right), \tag{20}$$

where $\boldsymbol{Q}_r(0)$ may not be a diagonal matrix in general since neither $\hat{x}_r$ nor $\hat{y}_r$ correspond to the principal complex curvature direction of the reflected beam wavefront. We diagonalize $\boldsymbol{Q}_r(0)$ to find its eigenvalues from

$$\begin{aligned}\lambda_{1,2} \;=\; & \frac{1}{\rho^r_{12} + \mathrm{j}b^r_{12}} = \frac{1}{2}(Q^r_{11} + Q^r_{22}) \\ & \pm\sqrt{(Q^r_{11} + Q^r_{22})^2 - 4\det(\boldsymbol{Q}_r(0))}. \end{aligned} \tag{21}$$

Then the principal direction (or eigenvector) for the reflected beam can be found from

$$\begin{aligned}\hat{X}_r &= \frac{(Q^r_{22} - \lambda_1)\hat{x}_r - Q^r_{12}\hat{y}_r}{\sqrt{(Q^r_{22} - \lambda_1)^2 + (Q^r_{12})^2}}, \\ \hat{Y}_r &= \frac{Q^r_{12}\hat{x}_r + (Q^r_{22} - \lambda_1)\hat{y}_r}{\sqrt{(Q^r_{22} - \lambda_1)^2 + (Q^r_{12})^2}}. \end{aligned} \tag{22}$$

It should be noted that the procedure of diagonalization follows

$$(\hat{x}_r\ \hat{y}_r)\boldsymbol{Q}_r(0)(\hat{x}_r\ \hat{y}_r)^{\mathrm{T}} = (\hat{X}_r\ \hat{Y}_r)\begin{bmatrix}\lambda_1 & 0\\ 0 & \lambda_2\end{bmatrix}(\hat{X}_r\ \hat{Y}_r)^{\mathrm{T}}. \tag{23}$$

This equation can be understood as $\boldsymbol{Q}_r(0)$ that can be diagonalized by rotating $(\hat{x}_r\ \hat{y}_r)$ into complex coordinate space $(\hat{X}_r\ \hat{Y}_r)$. It is very convenient to directly track the beam with the complex phase $\boldsymbol{Q}$ matrix, and the reflected field can be easily obtained from Eq. (7).

By the way, most of the obstacles in the environment have flat structures. As depicted in Fig. 2(b), a beam illuminates on a flat surface, the local principal radii of curvature of the surface $R_1$ and $R_2$ become infinite. While the formula derived above is still true, it is just like an incoming wave emitted from the position of the mirror point of the flat.

## 4. Calculation of multi-reflection field

The total field is determined via coherent superposition of the individual contributions of each beam. The complex field of the $i$-th beam at the receiver is given by

$$\begin{aligned}&\psi_r(x_n, y_n, z_n) \\ &= \psi_i^0 \cdot \prod_j \bar{\bar{R}}_{E,H} \cdot \sqrt{\frac{\det\boldsymbol{Q}(z_0)}{\det\boldsymbol{Q}(0)}} \cdot \sqrt{\frac{\det\boldsymbol{Q}_1(z_1)}{\det\boldsymbol{Q}_1(0)}} \cdots \\ &\quad \sqrt{\frac{\det\boldsymbol{Q}_{n-1}(z_{n-1})}{\det\boldsymbol{Q}_{n-1}(0)}} \cdot \sqrt{\frac{\det\boldsymbol{Q}_n(z_n)}{\det\boldsymbol{Q}_n(0)}} \cdot \exp\left(-\mathrm{j}k\sum_{j=0}^{n} z_j\right) \\ &\quad \times \exp\left\{-\frac{\mathrm{j}k}{2}[(x_n\ y_n)\boldsymbol{Q}_n(z_n)(x_n\ y_n)^{\mathrm{T}}]\right\}. \end{aligned} \tag{24}$$

It is noted that each reflection needs to change the coordinate system, and the origin of the new coordinate system is located at the intersection point. The $\bar{\bar{R}}_{E,H}$ defined in Eq. (24) is the dyadic planar reflection coefficient which is given by

$$\bar{\bar{R}}_E = -\hat{e}^i_\perp\hat{e}^r_\perp + \hat{e}^i_\parallel\hat{e}^r_\parallel, \quad \bar{\bar{R}}_H = \hat{e}^i_\perp\hat{e}^r_\perp - \hat{e}^i_\parallel\hat{e}^r_\parallel, \tag{25}$$

where

$$\begin{cases}\hat{e}^i_\perp = \dfrac{\hat{z}_i \times \hat{z}}{\sin\theta_i}, \\ \hat{e}^i_\parallel = \hat{e}^i_\perp \times \hat{z}_i, \end{cases} \quad \text{and} \quad \begin{cases}\hat{e}^r_\perp = \dfrac{\hat{z}_r \times \hat{z}}{\sin\theta_i}, \\ \hat{e}^r_\parallel = \hat{e}^r_\perp \times \hat{z}_r. \end{cases} \tag{26}$$

## 5. Numerical examples and discussion

The purpose of this paper is to provide an improved ray model scheme for CSB tracking. Actual test data are not given here in this paper. However, in order to validate the correctness of the conclusion above, some numerical examples are given in this section. Then the algorithm results are compared with the simulation software, thereby proving the validity of the conclusion.

The first case of interest is the reflection of the CSB incident on a parabolic surface as shown in Fig. 3. Here, the CSB axis crosses the reflector surface at points $Q_1$ and $Q_2$ on the surface with the $x$ and $y$ coordinate of (0 m, 0 m) and (0.5 m, 0 m). It is noted that the local principal radii of curvature at these two point are different, and it is suitable to verify that the CSB is transformed into the reflected beam at the reflector surface. The CSB is located at the focus point with parameter $b = 5$ m, the focal length $f = 1$ m, and the diameter of the reflector $D = 2$ m. The simulation frequency is 15 GHz.

Figure 4 shows the comparison between the reflected field via CSB-GO in Eq. (7) and the General Reflector Antenna Software Package (GRASP) in both $\varphi = 0^\circ$ and $\varphi = 90^\circ$ plane at $Q_1$ and $Q_2$ on the surface, respectively, with the radial distance $r = 1000$ m. It is obtained that these two incidence scenarios are in good agreement.

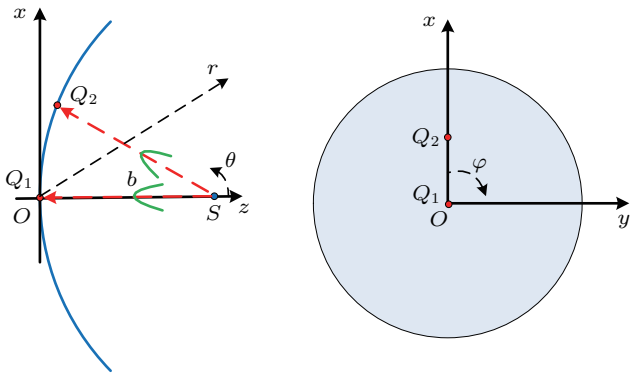



**Fig. 3.** (color online)Incident CSB illumination from the focus on a parabolic surface with beam axis hitting points $Q_1$ and $Q_2$ on the surface.

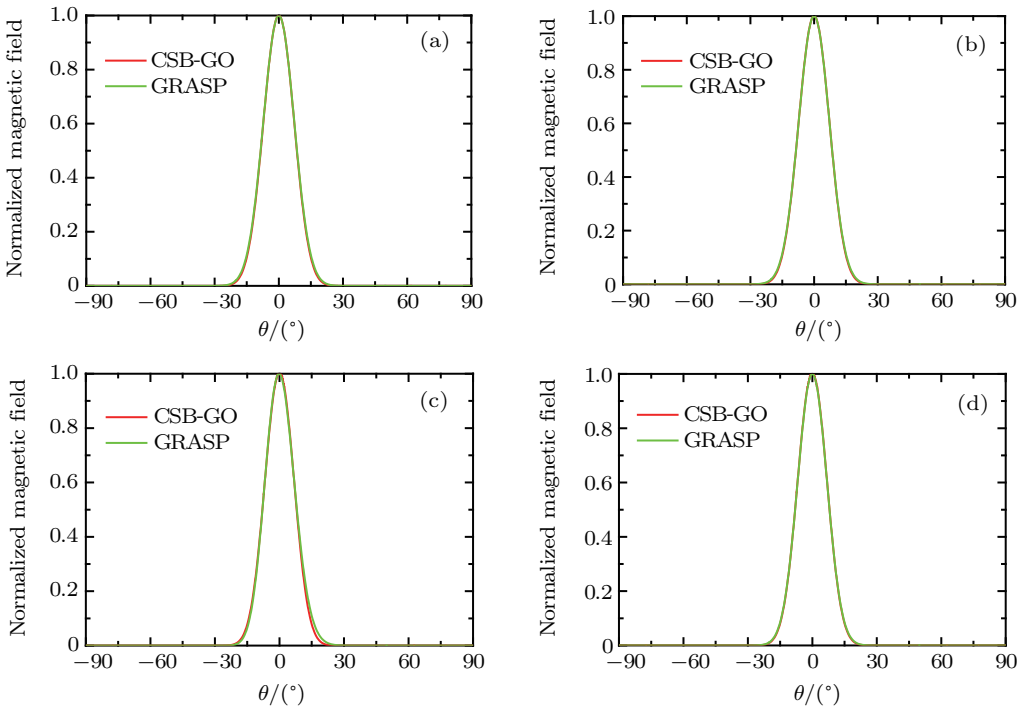



**Fig. 4.** (color online) Comparisons between the reflected field via CSB-GO in Eq. (7) and the GRASP, respectively, in (a) $\varphi = 0^\circ$ plane at $Q_1$, (b) $\varphi = 90^\circ$ plane at $Q_1$, (c) $\varphi = 0^\circ$ plane at $Q_2$, and (d) $\varphi = 90^\circ$ plane at $Q_2$.

In order to verify the total field of the reflector illuminated by a feed horn given in Ref. [9], the radiation magnetic field of the horn is expanded in terms of CSBs, then the total field is determined via coherent superposition of the individual contributions of each beam with local approximation at each reflection point. The relevant parameters are given in the first case. The feed is located at the focus point and the axis of the horn points to the center of the reflector. The observation point is $r = 1000$ m in the global coordinate system. The normalized magnetic field in the $\varphi = 0^\circ$ plane is depicted in Fig. 5(a) and in the $\varphi = 90^\circ$ plane is described in Fig. 5(b). Due to the co-polarization being much larger than the cross-polarization, only the $\theta$ component in the $\varphi = 0^\circ$ plane, and the $\varphi$ component in the $\varphi = 90^\circ$ plane are present. The proposed CSB-GO method and the GRASP in the main lobe region are shown to be in good agreement with each other. Since the proposed CSB-GO method is performed in the paraxial regions, where most of the contribution of the reflection is in the neighborhood of the reflection point, and thus resulting in some differences between these two results outside the main lobe region.

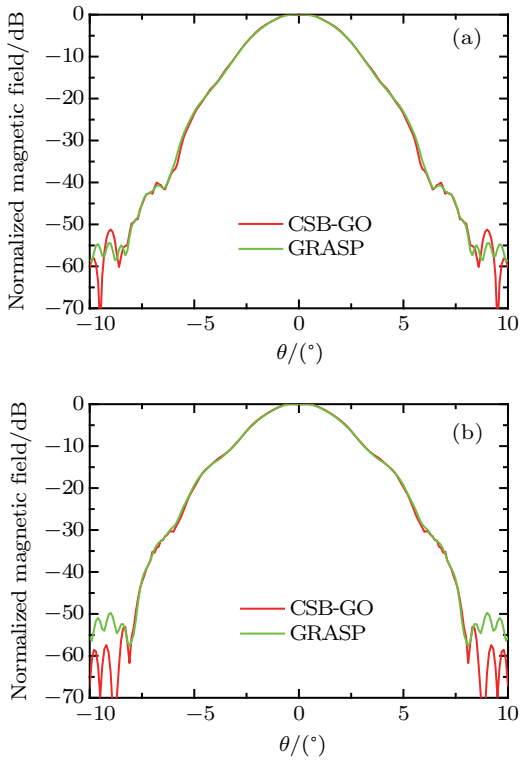



**Fig. 5.** (color online) Comparisons between the plots of the normalized magnetic fields of CSB-GO and GRASP versus $\theta$, showing (a) $\theta$ component in the $\varphi = 0^\circ$ plane and (b) $\varphi$ component in the $\varphi = 90^\circ$ plane.

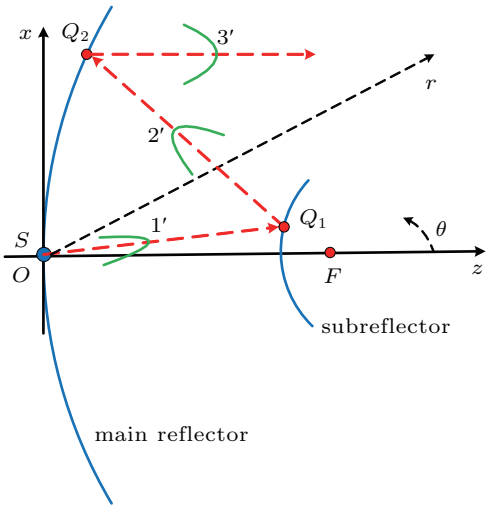



**Fig. 6.** (color online) Structure of multi-reflection.

In order to compare with the result of the existing simulation software GRASP, a simple double reflector surface is presented as the last case to verify the multi-reflection condition. The CSB is located at the virtual focus of the subreflector with parameter $b = 10$ m. The diameter of the main reflector $D$ is 2.4 m, and its focal length is 0.8 m, the diameter of the subreflector $d$ is 0.74 m, and its focal length is 0.4 m. The simulation frequency is 15 GHz. As depicted in Fig. 6, for the CSB emission from the focus, the first reflection happens in the subreflector, then the first reflected beam contacting the main reflector experiences the secondary reflection. Figures 7(a) and 7(b) show the comparisons between the multiply reflected field via CSB-GO in Eq. (7) and the GRASP in both $\varphi = 0^\circ$ plane and $\varphi = 90^\circ$ plane, respectively, with the radial distance $r = 1000$ m. The results obtained from Figs. 7(a) and 7(b) are in good agreement with each other.

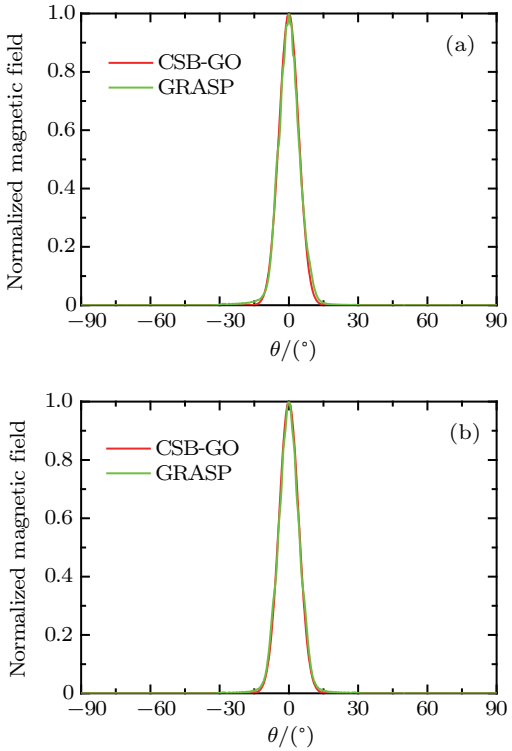



**Fig. 7.** (color online) Comparisons between the plots of the normalized magnetic fields of CSB-GO and GRASP versus $\theta$, showing (a) $\theta$ component in the $\varphi = 0^\circ$ plane, and (b) $\varphi$ component in the $\varphi = 90^\circ$ plane.

## 6. Conclusions

In this paper, an improved ray model scheme for the CSB tracking technique is presented. The CSB basis function has a Gaussian-type amplitude distribution and is suitable for replacing a GO ray tube in the ray tracing approach. A complex phase matching technique is adopted to find the reflected beam at the reflection point. Local approximation is used to represent the curved surface near the reflection point. A conventional right-handed reflection system is used to track the field easily. It is a promising method of analyzing the electromagnetic characteristics of the complex environment in the future.

## References

[1] Austin A, Neve M and Rowe G 2011 *IEEE Trans. Anten. Propag.* **59** 4239

[2] Castro B, Gomes I, Ribeiro F and Cavalcante G 2010 *European Conference on Antenna and Propagation IEEE*, April 2010, Barcelona, Spain, p. 1

[3] Nisirat M A, Ismail M, Nissirat L, Alkhwaldeh S and Yuwono T 2011 *International Conference on Telecommunication System, Services, and Applications IEEE*, October 2011, Indonesia, p. 284

[4] Tiberi G, Bertini S, Malik W Q, Monorchio A, Edwards D J and Manara G 2016 *IEEE Trans. Anten. Propag.* **57** 777

[5] Yun Z Q, Zhang Z J and Iskander M F 2002 *IEEE Trans. Anten. Propag.* **50** 750

[6] Yao R, Gao G, Chen Z and Zhu W 2003 *IEEE Global Telecommunications Conference*, December 2003, San Francisco, California, p. 1205

[7] Yao R, Zhu W and Chen Z 2003 *IEEE Vehicular Technology Conference*, October 2003, Orlando, Florida, p. 1293

[8] Seidel S Y and Rappaport T S 1994 *IEEE Transaction on Vehicular Technology* **43** 879

[9] Gao M, Yang F, Yan F and Zhou L J 2017 *Electromagnetics* **37** 1

[10] Zhu Q, Ren J, Xu D, Chen X, Yu X and Tang Y 2013 *IEEE International Conference on Communication*, June 2013, Budapest, Hungary, p. 186

[11] Kouyoumjian R G and Pathak P H 1974 *Proc. IEEE* **62** 1448

[12] Heyman E and Felsen L B 2001 *J. Opt. Soc. Am. A* **18** 1558